EasyChair Preprint

№ 15389

# A Numerical Parameter Optimization Design Method for Isolated Tripe Active Bridge Converter

Qinwei Zhang, Jia Li and Ruping Cen



November 7, 2024

# A Numerical Parameter Optimization Design Method For Isolated Tripe Active Bridge Converter

Qinwei Zhang
*College of Automation*
*Chongqing University of Posts and Telecommunications*
Chongqing, China
zqw1076488925@126.com

Jia Li
*College of Automation*
*Chongqing University of Posts and Telecommunications*
Chongqing, China
jiali@cqupt.edu.cn

Ruping Cen
*College of Automation*
*Chongqing University of Posts and Telecommunications*
Chongqing, China
cenruping@cqupt.edu.cn

***Abstract*—To enhance the operational efficiency of multi-port converters across their entire working range, this paper proposes a numerical parameter optimization design method based on hierarchical constraints. We provide a detailed analysis of the working principle of the isolated three-active-bridge converter and establish a frequency-domain steady-state analysis model. Building on this foundation, we sequentially introduce constraints such as voltage gain, maximum power, and Zero Voltage Switching (ZVS) alongside the converter's operating characteristics and safe operating domain. This approach significantly reduces the parameter design space and simplifies the optimization process. Next, we optimize the main circuit parameters of the multi-port converter with the objective of minimizing the weighted average loss across the full operating range. Our proposed method takes into account the complex coupling of the main circuit parameters, thereby avoiding efficiency degradation that can arise from overlooking these interactions. Moreover, the optimization process is grounded in the full operating domain, ensuring efficient performance across various loads and operating conditions.**

***Keywords—Multiport converter, Isolated three active bridge converter, DC-DC converter, Parameter design, Efficiency***

## I. INTRODUCTION

In independent new energy power generation systems, such as DC microgrids and aerospace power systems, it is often necessary to equip an energy storage device. This serves as an energy buffer unit to manage the intermittency and randomness of new energy generation. Such measures ensure the stability and continuity of the power supply. [1-2]

Unlike multiple two-port converters, a single multi-port converter enables power transmission and control among several ports through a more integrated approach. This offers key advantages. These include fewer power conversion links, greater integration, and improved efficiency [3]. Consequently, multi-port converters have been widely adopted in fields like DC microgrids, electric vehicles, and energy storage [4-6]

However, the increasing complexity of application scenarios and the diversity of multi-port converter structures pose significant challenges. Fully leveraging their performance advantages is not straightforward. This includes not only selecting the appropriate converter topology but also tackling the intricacies of parameter design.

Once the converter topology is established, the parameter design of the main circuit directly influences the converter's steady-state performance limits. It plays a crucial role in key metrics such as voltage regulation, power transmission efficiency, and soft switching characteristics. Therefore, precise parameter design can enhance the overall performance of the converter. It also ensures that the converter meets expectations in real-world applications.

In literature [7,8], researchers conducted numerical efficiency optimization for a single-phase dual-boost PFC rectifier. They achieved an impressive experimental efficiency of 99.1% at a power density of 1.1 kW/dm³. They defined the feasible energy space for high efficiency and low power density based on a mathematical model. Additionally, they identified the multi-objective compromise limit curve of efficiency versus power density (the Pareto frontier). Through their optimization program, they successfully automated the design of PFC parameter values. Similarly, literature [9] describes the automatic parameter design of a phase-shifted PWM DC-DC converter. The prototype achieved 99.2% power transmission efficiency and a power density of 36 W/in³ under full load conditions. Reference [10] also evaluates the impact of novel SiC devices on the system-level performance of PFC converters, including efficiency and power density, through numerical analysis and optimization techniques.

However, most research on parameter design has focused primarily on two-port converters [11,12]. There are limited studies addressing the optimization of main circuit parameters in multi-port converters. Multi-port converters require more design parameters. These include the high-frequency transformer turn ratio and the power inductance value for each port—typically at least six design parameters. These parameters are significantly interdependent. This makes it challenging to identify an optimal combination based solely on maximum power transfer requirements and voltage gain, as is common with dual active full bridges. Most literature [13,14] merely correlates the maximum transfer power with the voltage and current demands of the multi-port converter. They select transformer turn ratios and inductance values somewhat arbitrarily, without adequately considering how hardware parameters affect the converter's steady-state performance.

To address these issues, this paper takes the typical Isolated Triple Active Bridge DC-DC converter as a case study. We propose a numerical parameter optimization design method grounded in hierarchical constraints. We conduct a comprehensive and systematic study on parameter design for multi-port converters. Our goal is to enhance their operational efficiency across the entire working range. A 2 kW experimental prototype platform is designed based on the parameter design results. The effectiveness and feasibility of the proposed design method are validated through both simulation and experimental tests.

## II. Steady State Analysis Modeling

### A. Equivalent circuit model

Fig. 1 illustrates the circuit topology of the ITAB converter, which has three ports connected through a three winding transformer and three H-bridge switching networks.

$N_1$:$N_2$:$N_3$ are the turns ratios of the three ports of the high-frequency transformer.$L_1$~$L_3$ is the sum of transformer leakage inductance and applied inductance. Since the excitation inductance of the transformer is much larger than the leakage inductance, the excitation inductance is assumed to be infinite. $S_1$~$S_4$, $Q_1$~$Q_4$ and $J_1$~$J_4$ denote the switching devices in the three H-bridges, which are composed of an active switch Tx, a parasitic capacitor $C_{ossx}$ and an anti-parallel diode Dx. $v_{h1}$~$v_{h3}$ are the AC square wave voltages generated by the three H-bridges. $i_{L1}$~$i_{L3}$ denote the instantaneous current values flowing through inductors $L_1$~$L_3$. $V_1$~$V_3$ and $i_1$~$i_3$ denote the terminal voltage and terminal current of the three ports, respectively. The reference direction is shown in Fig. 1.

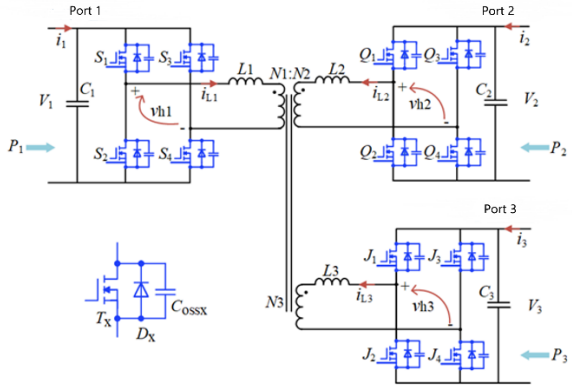


Fig. 1. Magnetically Integrated Isolated Triple Active Bridge DC-DC Converter

### B. Steady state analysis model in frequency domain

This paper will use the frequency domain analysis method to establish a unified mathematical model of ITAB converter. First, the voltage gain of the ITAB converter is defined as:

$$M_{12}=\frac{n_{12}V_2}{V_1};\quad M_{13}=\frac{n_{13}V_3}{V_1};\quad M_{23}=\frac{n_{12}V_2}{n_{13}V_3}$$

The reference current and power of the ITAB converter are defined as:

$$I_N=\frac{4V_1}{\pi\omega_s L_1};\qquad P_N=\frac{8V_1^2}{\pi^2\omega_s L_1};$$

Based on Fourier series decomposition, the AC square wave voltage $v_{h1}$~$v_{h3}$ of the full bridge output can be decomposed into:

$$\begin{cases} v_{h1}=\sum\limits_{n=1,3,5...}^{\infty}\frac{4V_1}{n\pi}\cos\left(n\frac{\alpha_1}{2}\right)\sin\left(n\omega_s t\right)\\ v_{h2}=\sum\limits_{n=1,3,5...}^{\infty}\frac{4V_2}{n\pi}\cos\left(n\frac{\alpha_2}{2}\right)\sin\left[n\left(\omega_s t-\varphi_{12}\right)\right]\\ v_{h3}=\sum\limits_{n=1,3,5...}^{\infty}\frac{4V_3}{n\pi}\cos\left(n\frac{\alpha_3}{2}\right)\sin\left[n\left(\omega_s t-\varphi_{13}\right)\right] \end{cases} \tag{1}$$

Where, angular frequency ωs=2πfs, fs represents the switching frequency of ITAB. Based on the equivalent circuit of Δ type, the standardized inductive current instantaneous value $i_{L1,N}$~$i_{L3,N}$ can be expressed as:

$$\begin{cases} i_{L1,N}(t)=i_{L1,N}(0)+\frac{1}{I_N}\left(\int_0^t\frac{v_{h1}-v_{h2}'}{L_{12}}dt-\int_0^t\frac{v_{h3}'-v_{h1}}{L_{13}}dt\right)\\ i_{L2,N}(t)=i_{L2,N}(0)+\frac{n_{12}}{I_N}\left(\int_0^t\frac{v_{h2}'-v_{h3}'}{L_{23}}dt-\int_0^t\frac{v_{h1}-v_{h2}'}{L_{12}}dt\right)\\ i_{L3,N}(t)=i_{L3,N}(0)+\frac{n_{13}}{I_N}\left(\int_0^t\frac{v_{h3}'-v_{h1}}{L_{13}}dt-\int_0^t\frac{v_{h2}'-v_{h3}'}{L_{23}}dt\right) \end{cases} \tag{2}$$

It can be seen from the working characteristics of the ITAB converter that the average value of the inductor current in a steady-state switching period is equal to 0, so we can get the following relationship:

$$i_{Li,N}(0)=-i_{Li,N}\left(\frac{\pi}{\omega_s}\right)\qquad i=1,2,3 \tag{3}$$

Substitute equation (2) into equation (3), and the instantaneous value expression of inductance current obtained by solving is as follows:

$$\begin{cases} i_{L1,N}(t)=\sum\limits_{n=1,3,5...}^{\infty}\frac{1}{n^2}\sqrt{A_1^2+B_1^2}\sin\left[n\omega_s t+\arctan\left(\frac{A_1}{B_1}\right)\right]\\ i_{L2,N}(t)=\sum\limits_{n=1,3,5...}^{\infty}\frac{n_{12}}{n^2}\sqrt{A_2^2+B_2^2}\sin\left[n\omega_s t+\arctan\left(\frac{A_2}{B_2}\right)\right]\\ i_{L3,N}(t)=\sum\limits_{n=1,3,5...}^{\infty}\frac{n_{13}}{n^2}\sqrt{A_3^2+B_3^2}\sin\left[n\omega_s t+\arctan\left(\frac{A_3}{B_3}\right)\right] \end{cases} \tag{4}$$

where $A_1$=$A_{12}$-$A_{13}$, $B_1$=$B_{12}$-$B_{13}$, $A_2$=$A_{23}$-$A_{12}$, $B_2$=$B_{23}$-$B_{12}$, $A_3$=$A_{31}$-$A_{23}$, $B_3$=$B_{31}$-$B_{23}$. The expressions of $A_{12}$, $B_{12}$, $A_{13}$, $B_{13}$, $A_{23}$ and $B_{23}$ are shown in equation (5).

$$\begin{cases} A_{12}=\frac{M_{12}\cos(n\varphi_{12})\cos(n\alpha_2/2)-\cos(n\alpha_1/2)}{(L_{12}/L_1)}\\ B_{12}=\frac{M_{12}\sin(n\varphi_{12})\cos(n\alpha_2/2)}{(L_{12}/L_1)}\\ A_{13}=\frac{\cos(n\alpha_1/2)-M_{13}\cos(n\varphi_{13})\cos(n\alpha_3/2)}{(L_{13}/L_1)}\\ B_{13}=\frac{-M_{13}\sin(n\varphi_{13})\cos(n\alpha_3/2)}{(L_{13}/L_1)}\\ A_{23}=\frac{M_{13}\cos(n\varphi_{13})\cos(n\alpha_3/2)-M_{12}\cos(n\varphi_{12})\cos(n\alpha_2/2)}{(L_{23}/L_1)}\\ B_{23}=\frac{M_{13}\sin(n\varphi_{13})\cos(n\alpha_3/2)-M_{12}\sin(n\varphi_{12})\cos(n\alpha_2/2)}{(L_{23}/L_1)} \end{cases} \tag{5}$$

$$\begin{cases} P_{1,\mathrm{N}}=\dfrac{1}{T_{\mathrm{s}}P_{\mathrm{N}}}\left[\int_0^{T_{\mathrm{s}}}v_{\mathrm{h1}}i_{\mathrm{L12}}dt-\int_0^{T_{\mathrm{s}}}v_{\mathrm{h1}}i_{\mathrm{L13}}dt\right]=\sum_{n=1,3,5\ldots}^{\infty}\dfrac{\cos(n\alpha_1/2)}{n^3}\left[M_{12}\sin(n\varphi_{12})\cos\left(n\dfrac{\alpha_2}{2}\right)/\left(\dfrac{L_{12}}{L_1}\right)-M_{13}\sin(n\varphi_{13})\cos\left(n\dfrac{\alpha_3}{2}\right)/\left(\dfrac{L_{31}}{L_1}\right)\right] \\ P_{2,\mathrm{N}}=\dfrac{1}{T_{\mathrm{s}}P_{\mathrm{N}}}\left[\int_0^{T_{\mathrm{s}}}v_{\mathrm{h2}}i_{\mathrm{L23}}dt-\int_0^{T_{\mathrm{s}}}v_{\mathrm{h1}}i_{\mathrm{L12}}dt\right]=\sum_{n=1,3,5\ldots}^{\infty}\dfrac{M_{12}\cos(n\alpha_2/2)}{n^3}\left[M_{13}\sin(n\varphi_{23})\cos\left(n\dfrac{\alpha_3}{2}\right)/\left(\dfrac{L_{23}}{L_1}\right)-\sin(n\varphi_{12})\cos\left(n\dfrac{\alpha_1}{2}\right)/\left(\dfrac{L_{12}}{L_1}\right)\right] \\ P_{3,\mathrm{N}}=\dfrac{1}{T_{\mathrm{s}}P_{\mathrm{N}}}\left[\int_0^{T_{\mathrm{s}}}v_{\mathrm{h3}}i_{\mathrm{L31}}dt-\int_0^{T_{\mathrm{s}}}v_{\mathrm{h2}}i_{\mathrm{L23}}dt\right]=\sum_{n=1,3,5\ldots}^{\infty}\dfrac{M_{13}\cos(n\alpha_3/2)}{n^3}\left[\sin(n\varphi_{31})\cos\left(n\dfrac{\alpha_1}{2}\right)/\left(\dfrac{L_{31}}{L_1}\right)-M_{12}\sin(n\varphi_{23})\cos\left(n\dfrac{\alpha_2}{2}\right)/\left(\dfrac{L_{23}}{L_1}\right)\right] \end{cases} \quad (6)$$

Combined with equation (4) and equation (5), the inductive current RMS value of the ITAB converter can be expressed as:

$$\begin{cases} I_{\mathrm{rms1,N}}=\dfrac{1}{n^2\sqrt{2}}\sqrt{A_1^{\,2}+B_1^{\,2}} \\ I_{\mathrm{rms2,N}}=\dfrac{n_{12}}{n^2\sqrt{2}}\sqrt{A_2^{\,2}+B_2^{\,2}} \\ I_{\mathrm{rms3,N}}=\dfrac{n_{13}}{n^2\sqrt{2}}\sqrt{A_3^{\,2}+B_3^{\,2}} \end{cases} \quad (7)$$

Similarly, according to formula (1) and (4), the transmission power of each port in a switching cycle can be derived, and its per unit value expression is shown in formula (7).

## III. PARAMETER OPTIMIZATION DESIGN

As shown in Fig.1, the parameter design space of ITAB converter includes six parameters: power inductance value $L_1$, $L_2$, $L_3$ and transformer turns $N_1$, $N_2$, $N_3$. To facilitate analysis, they are normalized below. Using $N_3$ as the base, the turns $N_1$ and $N_2$ of ports 1 and 2 can be normalized to $n_{12}$ and $n_{13}$. Then, taking $L_1$ as a reference, the relationship shown in equation (8) can be derived, thereby normalizing the inductors $L_2$ and $L_3$ to $k_{12}$ and $k_{13}$.

$$\begin{cases} k_{12}=\dfrac{n_{12}^{\,2}L_2}{n_{13}^{\,2}L_3}+\dfrac{n_{12}^{\,2}L_2}{L_1}+1 \\ k_{13}=\dfrac{n_{13}^{\,2}L_3}{n_{12}^{\,2}L_2}+\dfrac{n_{13}^{\,2}L_3}{L_1}+1 \end{cases} \quad (8)$$

Through normalization, the parameters in the parameter design space are converted into $L_1$, $k_{12}$, $k_{13}$, $n_{12}$ and $n_{13}$. Theoretically, the parameter design space is infinite. In order to narrow the parameter optimization range and speed up the optimization speed, voltage gain constraints, inductance range constraints, maximum transmission power constraints and ZVS operating constraints are introduced in order to reduce the parameter design space based on ITAB operating characteristics, safe working domain and performance requirements.

### A. Constraining $n_{12}$ and $n_{13}$ based on voltage gain requirements

For power electronic converters, the closer the voltage gain approaches 1, the smaller the reflux power and loop current, and the higher the power transmission efficiency. [15]. According to the above rules, the voltage gain range of ITAB converter is set as $M_{12}\in[0.5, 1.3]$ and $M_{13}\in[0.8, 1.2]$ in this section, so as to exclude the parameter combination with large reactive power. The $M_{12}$ voltage gain is set to a wide range due to the wide voltage variation in port 2. Then, based on the above voltage gain range and gain expression, the design range of turn ratio $n_{12}$ and $n_{13}$ can be solved. So far, the range of parameters $n_{12}$ and $n_{13}$ has been successfully reduced to $n_{12}\in[0.9, 1.3]$, $n_{13}\in[2.7, 3.4]$ according to the voltage gain constraint.

### B. Based on the requirements of the inductance range, constrain $k_{12}$ and $k_{13}$

To consider the practical engineering application, limited by the winding process, the winding of the three ports of the transformer has a certain amount of leakage. Considering that the voltage of port 3 is small, the corresponding number of turns is relatively small. Therefore, the power inductance ranges of the three ports are limited to $L_1\geq4\mu$H, $L_2\geq4\mu$H, and $L_3\geq2\mu$H, respectively. According to equations (8), the functional relations of $L_2$ and $L_3$ for $L_1$, $k_{12}$, and $k_{13}$ can be written as:

$$\begin{cases} L_2=-\dfrac{L_1k_{12}+L_1k_{13}-L_1k_{12}k_{13}}{k_{13}n_{12,\max}^{\,2}}\geq4\mu\mathrm{H} \\ L_3=-\dfrac{L_1k_{12}+L_1k_{13}-L_1k_{12}k_{13}}{k_{12}n_{13,\max}^{\,2}}\geq2\mu\mathrm{H} \end{cases} \quad (9)$$

The effective design space of parameters $k_{12}$ and $k_{13}$ can be solved by combining the formula (9). Because the $k_{12}$ and $k_{13}$ ranges are related to $L_1$, the numerical ranges of $k_{12}$ and $k_{13}$ cannot be given directly.

### C. Constraining $L_1$, $k_{12}$ and $k_{13}$ based on the maximum transmission powe requirements

To create multileveled equations, it may be necessary to treat the equation as a graphic and insert it into the text after your paper is styled. Considering a certain overload capacity, the maximum transmission power range of the three ports of the ITAB converter should meet the requirements of $|P_{1,\max}|\geq5$kW, $P_{2,\max}\geq4$kW, $|P_{3,\max}|\geq4$kW. That is, $P_{1,\max}$, $P_{2,\max}$ and $P_{3,\max}$ and the constraint relation of max on $k_{12}$ and $k_{13}$ is:

$$\begin{cases} \left|P_{1,\max}\right|=\left|\sum_{n=1,3,5\ldots}^{11}\dfrac{1}{n^3}\left(\dfrac{M_{12,\min}}{k_{12}}+\dfrac{M_{13,\min}}{k_{13}}\right)\right|\geq5000\mathrm{W} \\ P_{2,\max}=\sum_{n=1,3,5\ldots}^{11}\dfrac{M_{12,\min}}{n^3}\left(\dfrac{M_{13,\min}}{k_{23}}+\dfrac{1}{k_{12}}\right)\geq4000\mathrm{W} \\ \left|P_{3,\max}\right|=\left|\sum_{n=1,3,5\ldots}^{11}\dfrac{M_{13,\min}}{n^3}\left(\dfrac{M_{12,\min}}{k_{23}}+\dfrac{1}{k_{13}}\right)\right|\geq4000\mathrm{W} \end{cases} \quad (10)$$

Fig.2 shows the effective design space for $k_{12}$ and $k_{13}$ when $L_1$ takes different values. It is found that with the increase of $L_1$, the parameter design space of $k_{12}$ and $k_{13}$ gradually decreases. When $L_1$=60μH, there is no design space to meet the maximum power requirements. Therefore, the

range of the design parameter $L_1$ should be constrained to $L_1 \in [4\mu H, 50\mu H]$.

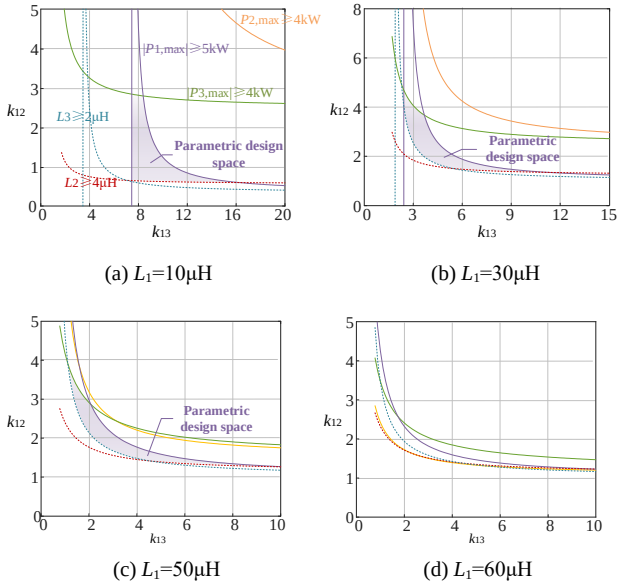


(a) $L_1$=10μH (b) $L_1$=30μH

(c) $L_1$=50μH (d) $L_1$=60μH

Fig. 2. Parameter design space of $k_{12}$ and $k_{13}$ under power transmission constraints

### D. Optimization of target parameters

Based on the previous constraints and analysis, we have narrowed the parameter design space down to a finite region. Although all parameters within this space can satisfy the design requirements of the converter and the maximum power requirements, different parameter combinations have varying impacts on the efficiency of the converter. Therefore, we still need to find an optimal parameters $[L_1, k_{12}, k_{13}, n_{12}, n_{13}]_{opt}$ with the objective of minimizing losses.

Due to ITAB's characteristics of having multiple operating modes and a wide power range in DC microgrid applications, we uniformly selected points at 20%, 50%, and 80% power in four different modes, resulting in a total of 72 typical operating points. The weighted average loss of these 72 operating points is taken as the final indicator to evaluate the performance of each group of parameters. By systematically comparing the weighted average losses corresponding to each group of parameters, we can ultimately determine an optimal parameter combination. This combination not only satisfies all the constraints mentioned above but also has the minimum power transmission loss.

To demonstrate the effectiveness of parameter optimization, two typical parameter combinations from the parameter space are selected for comparative analysis against the optimal parameter combination. The specific numerical values of the three parameter sets are shown in Table I.

TABLE I. THREE SETS OF TYPICAL PARAMTETRS

| Circuit parameter combinations | *Parameter combination* $[L_1, k_{12}, k_{13}, n_{12}, n_{13}]$ | $L_2$ | $L_3$ |
|---|---|---|---|
| Optimal parameters | [40μH、3.2、3.0、1.1、2.7] | 38μH | 6μH |
| Typical parameters 1 | [10μH、2.2、8.0、0.9、3.3] | 12μH | 3μH |
| Typical parameters 2 | [50μH、1.8、4.0、1.3、2.7] | 10μH | 5μH |

## IV. EXPERIMENTAL VALIDATION

In order to verify the validity of the above theory and simulation analysis, the two sets of parameters, typical parameters 1 and optimal parameters, are experimentally tested respectively, and their steady-state performance is fully analyzed and compared.

Fig.3 is the experiment platform. The prototype samples the voltage and current of the port through two independent isolated current sampling chip AMC1301, and the sampling results obtained are fed into the AD interface of the digital signal processor TMS320F28335 for analog-to-digital conversion, and programmed to realize closed-loop control in the TMS320F28335.

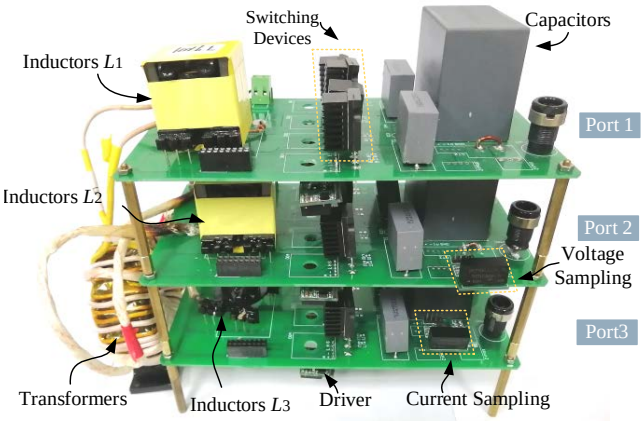


Fig. 3. The experiment platform of the IITAB converter

### A. Steady state operating waveform

Here, two typical working points are selected for experimental testing and analysis. Fig.4 shows the typical operating waveforms for $P_1$=$P_3$=−300W when the port voltage $V_1$=380V, $V_2$=360V, $V_3$=132V respectively.

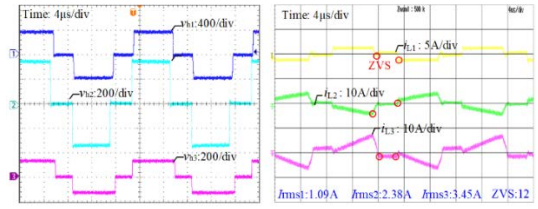


(a) Optimal parameter combination

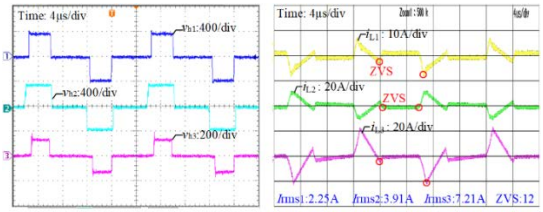


(b) Typical parameter combination 1

Fig. 4. Parameter Typical working waveforms at $V_1$=380V，$V_2$=360V，$V_3$=132V，$P_1$=$P_3$=−300W

As shown in Fig.4, the inductor current RMS corresponding to the optimal parameter combination are 1.09A, 2.38A and 3.45A respectively, which are basically consistent with the theoretical calculation of 1.11A, 2.31A and 3.22A. Compared with typical parameters 1, the current values of the three ITAB ports are reduced by about 50% under the optimized parameters.

### B. *Efficiency of experimental testing*

Fig. 5 shows how the conversion efficiency of the ITAB converter varies with power. The blue and orange curves represent the experimental efficiency values under the optimal parameter parameters and the typical parameters, respectively.

Compared with the measured efficiency curve of typical parameters 1, the efficiency curve of optimal parameter combination is significantly improved in the whole power range. The weighted average efficiency of the two groups of circuit parameters is 96.08% and 97.48%, respectively. Through parameter optimization design, the transformation efficiency of ITAB is improved by approximately 1.5% overall.

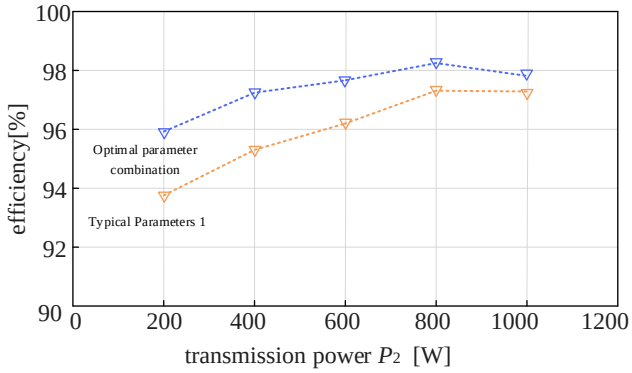


Fig. 5. The efficiency curves of optimal and typcal parameters

## V. Conclusions

To enhance operational efficiency across the entire working domain, this paper proposes a numerical parameter design method based on the concept of hierarchical constraints. Initially, we introduce constraints related to voltage gain, inductance range, and maximum transmission power according to the design requirements. By systematically constraining all critical circuit parameters, we significantly reduce the parameter optimization range. Next, we establish the power loss model for the ITAB and define the mapping relationship between the design space and the performance space. Building on this foundation, we complete the parameter optimization design for the ITAB, aiming to minimize the weighted average loss across the converter's entire working domain. This process allows us to determine the optimal circuit parameter combination for the DC microgrid operational scenario. To validate the effectiveness of the proposed parameter design method, we select one optimal parameter combination along with two sets of typical parameter combinations for simulation and experimental verification. The results indicate that under the experimental conditions, the optimized parameter combination yields an approximate 1.5% increase in the average efficiency of the ITAB switching devices across the entire working domain.

## References


[1] Zhao Xianhao, Xie Hongfu, Liu Fei, et al. Research and Application of Building DC Microgrid Based on Multi-port Power Router [J]. Electrical Technology, 2022, 23(08): 75-83.

[2] Zhang Xiangyu, Shu Yinan, et al. Multi-time scale energy optimization and zonal coordinated control of source-load-storage in DC microgrid based on virtual energy storage[J]. Transactions of China Electrotechnical Society, 2022, 37(23): 6011-6024.

[3] Song Xin, Xiao Jianguo, et al. A phase-shift controlled three-port DC-DC converter for hybrid renewable energy generation [J]. Transactions of China Electrotechnical Society, 2015, 30(17): 36-44.

[4] Hebala, Osama M, Aboushady, et al. Generalized active power flow controller for multiactive bridge DC-DC converters with minimum current point tracking algorithm[J]. IEEE Transactions on Industrial Electronics, 2022, 13(4):3764-3775.

[5] Pereira T, Hoffmann F, et al. A comprehensive assessment of multiwinding transformer-Based DC-DC converters[J].IEEE Transactions on Power Electronics, 2021, 36(9): 10020-10036.

[6] P. Wang, X. Lu, W. Wang and D. Xu, Frequency division based coordinated control of three-Port converter interfaced hybrid energy storage systems in autonomous DC microgrids," in IEEE Access, 2018, 6, 25389-25398.

[7] Kolar J W, Biela J, Minibock J. Exploring the pareto front of multi-objective single-phase PFC rectifier design optimization-99.2% efficiency vs. 7kW/din 3 power density[C]. IEEE International Power Electronics and Motion Control Conference, 2009, 1-21.

[8] Biela J, Kolar J W, Deboy G. Optimal design of a compact 99.3% efficient single-phase PFC rectifier[C]. IEEE Applied Power Electronics Conference and Exposition, 2010, 1397-1404.

[9] Badstuebner U, Biela J, Kolar J W. Design of an 99%-efficient, 5kW, phase-shift PWM DC-DC converter for telecom applications[C]. IEEE Applied Power Electronics Conference and Exposition, 2010, 773-780.

[10] Biela J, Schweizer M, Waffler S, et al. SiC vs. Si-evaluation of potentials for performance improvement of power electronics converter systems by SiC power semiconductors[C]. Materials Science Forum, 2010, 1101-1106.

[11] Liu Zan, Sha Jin, Qiu Gaofeng, et al. Principle, Parameter Design, and Performance of a Multilevel Discrete Extended Phase-Shift Controlled Dual-Active-Bridge DC-DC Converter [J]. Transactions of China Electrotechnical Society, 2024, 39(12): 3761-3773.

[12] Huang Hewei, Cao Taiqiang, Pan Guangxu, et al. Parameter optimization design of a full-bridge CLL resonant converter considering the circulating power factor [J]. Transactions of China Electrotechnical Society, 2023, 38(20): 5503-5514.

[13] He Yifei. Research on on-board three-port converter with integrated OBC-LDC function [D]. Harbin Institute of Technology, 2020.

[14] P. Wang, X. Lu, W. Wang and D. Xu, Hardware decoupling and autonomous control of series- resonance-based three-port converters in DC microgrids[J]. IEEE Transactions on Industry Applications, 2019, 55(4):3901-3914.

[15] Zhao B, Song Q, Liu W, et al. Universal high-frequency-link characterization and practical fundamental-optimal strategy for dual-active-bridge DC-DC converter under PWM plus phase-shift control[J]. IEEE Transactions on Power Electronics, 2015, 30(12): 6488-6494.